

# Identification of active sites in CO oxidation and water-gas shift over supported Pt catalysts

Kunlun Ding,<sup>1</sup> Ahmet Gulec,<sup>2</sup> Alexis M. Johnson,<sup>1</sup> Neil M. Schweitzer,<sup>3</sup> Galen D. Stucky,<sup>4</sup> Laurence D. Marks,<sup>2</sup> Peter C. Stair<sup>1,5\*</sup>

<sup>1</sup>Department of Chemistry, Northwestern University, Evanston, IL 60208, USA. <sup>2</sup>Department of Materials Science and Engineering, Northwestern University, Evanston, IL 60208, USA. <sup>3</sup>Department of Chemical and Biological Engineering, Northwestern University, Evanston, IL 60208, USA. <sup>4</sup>Department of Chemistry and Biochemistry, University of California, Santa Barbara, CA 93106, USA. <sup>5</sup>Chemical Sciences and Engineering Division, Argonne National Laboratory, Argonne, IL 60439, USA.

\*Corresponding author. E-mail: pstair@northwestern.edu

**Identification and characterization of catalytic active sites are the prerequisites for an atomic level understanding of the catalytic mechanism and rational design of high-performance heterogeneous catalysts. Indirect evidences in recent reports suggest that Pt single atoms are exceptionally active catalytic sites. We demonstrate that infrared spectroscopy can be a fast and convenient characterization method to directly distinguish and quantify Pt single atoms from nanoparticles. In addition, we directly observe that only Pt nanoparticles show activity for CO oxidation and water-gas shift at low temperatures, while Pt single atoms behave as spectators. The lack of catalytic activity of Pt single atoms can be partly attributed to the strong binding of CO molecules.**

Low temperature catalytic conversions of CO to CO<sub>2</sub> via oxidation and water-gas shift (WGS) reactions are integral to several important processes, including the removal of CO from H<sub>2</sub> for fuel cell applications (1, 2) and emission control in automobiles with catalytic converters (3). Supported noble metal based catalysts, mainly Pt and Au, have been intensively studied for the reactions during the past decade because of their excellent activity and stability at low reaction temperatures. However, the reaction mechanisms are still highly debated, especially regarding the active site structures—single atoms (4–10) versus small Pt and Au nanoparticles (NPs) (11–16). For instance, there have been disagreements on the promotional effects of alkali cations in CO oxidation (17–20) and WGS (5, 10, 16, 21) reactions over supported Pt and Au catalysts. Some researchers attributed the promotional effects to the increased dispersion and activity of Pt and Au single atoms (5, 10); others correlated it to the increased activity of Pt and Au NPs (16–21). These differences in reaction mechanisms and identification of active sites may have arisen from conclusions drawn from techniques that either provide statistically limited information such as microscopy, or sample-averaged information such as x-ray absorption spectroscopy. More importantly, a direct observation of the catalytic performance of specific sites has long been lacking.

Site-specific techniques that provide statistically sufficient information on site identification and quantification as well as the activity evaluation of specific sites would make substantial progress toward resolving these discrepancies. Infrared (IR) spectroscopy of CO on supported noble metal catalysts is widely used because of its sensitivity to the atomic and electronic structures of the binding sites (22–24). Work done by Yates *et al.* on TiO<sub>2</sub> supported Au NPs showed that IR spectroscopy could identify the active site in CO oxidation (25) and that CO oxidation occurred within a zone at the perimeter of Au NPs surrounded by TiO<sub>2</sub> surface. Here, we show that IR spectroscopy with CO as a probe molecule can differentiate and quantify both Pt single atoms and NPs. We confirm the coexistence of Pt single atoms and NPs in many conventional catalysts and we observe that only the CO molecules adsorbed on Pt NPs can

react at low temperatures upon O<sub>2</sub> or H<sub>2</sub>O exposure. Thus, the active sites in CO oxidation and WGS reactions are present on the NPs but not on single atoms.

CO molecules were adsorbed on a series of Pt catalysts with varying ratios of Pt single atoms to NPs to investigate the corresponding changes to the IR absorption bands. Mesoporous zeolite HZSM-5 (Si/Al ratio of 62, morphology shown in fig. S1) (26) was chosen as the catalyst support because Al atoms are strictly isolated in the zeolite framework (27), providing isolated binding sites for Pt. The mesoporous structure is introduced to facilitate the diffusion of an organometallic Pt precursor, trimethyl(methylcyclopentadienyl)platinum (MeCpPtMe<sub>3</sub>), to the Al sites. Pt was loaded on the mesoporous HZSM-5 via either solution grafting at room temperature or vapor deposition at elevated temperatures (26).

The IR spectra of adsorbed CO on four Pt/HZSM-5 samples with different loadings (Fig. 1A) reveal two sets of CO absorption bands centered at 2115 cm<sup>-1</sup> and 2070 to 2090 cm<sup>-1</sup>. Adsorbed CO was not present on the bare zeolite HZSM-5 sample under our experimental conditions (fig. S2), indicating that these two peaks originate from CO molecules adsorbed on two different Pt species. We assigned the IR peak at 2070 to 2090 cm<sup>-1</sup> to CO molecules linearly adsorbed in an a-top geometry on Pt<sup>0</sup> atoms on single crystal

or NP surfaces (28–30). The relative intensity of the IR peak at 2070 to 2090  $\text{cm}^{-1}$  increased with the Pt loading, consistent with the increasing amount of Pt NPs on the zeolite support as observed by TEM (figs. S3 and S4). In addition, the red-shift of the IR peak at 2070 to 2090  $\text{cm}^{-1}$  during desorption (Fig. 1B and fig. S5) correlated with changes in dipole-dipole coupling between CO molecules on a Pt crystal surface (28–30).

A 0.5 wt % Pt/HZSM-5 sample, prepared from room temperature solution grafting, displayed several CO peaks in the polycarbonyl region (31, 32) (Fig. 1C). These peaks gradually decreased in intensity as the temperature increased during the desorption process (Fig. 1C) and a new peak at 2115  $\text{cm}^{-1}$  emerged and eventually became the only peak in the spectrum. The peak transformation was reversed upon re-exposure to CO (fig. S6). These trends indicate that cationic  $\text{Pt}^{\delta+}$ -polycarbonyl species formed initially upon CO exposure, before transforming into  $\text{Pt}^{\delta+}$ -monocarbonyl upon purging and heating. The cationic nature of grafted Pt was confirmed by x-ray photoelectron spectroscopy (XPS) (fig. S7). Compared to the absorption band from CO bonded to  $\text{Pt}^0$  NPs, the CO band assigned to  $\text{Pt}^{\delta+}$ -monocarbonyl is less red-shifted from the gas phase value (2143  $\text{cm}^{-1}$ ) because of decreased Pt d-electron back-donation to the CO  $\pi^*$  antibonding orbital. At short electron beam exposures, TEM (fig. S3) verified that Pt NPs were not present on the 0.5 wt % Pt/HZSM-5 sample prepared from room temperature solution grafting, as expected for the absence of the 2070–2090  $\text{cm}^{-1}$  peak. However, the zeolite structures decomposed in the electron beam within 1 min, leading to the appearance of Pt NPs. The poor stability under electron beam exposure hinders the high-angle annular dark-field (HAADF) imaging of Pt species with atomic resolution in zeolites. In order to avoid the degradation of the support, we used Al-doped amorphous silica as the support. A 0.6 wt % Pt/ $\text{SiO}_2(\text{Al})$  sample prepared from room temperature solution grafting gave similar CO IR spectra to that of 0.5 wt % Pt/HZSM-5 sample (fig. S8). Aberration-corrected HAADF images show that the Pt was dispersed on the surface predominantly as isolated single atoms (Fig. 1F and figs. S9 and S10).

Based on the IR, TEM, and XPS results, we assigned the IR bands centered at 2115  $\text{cm}^{-1}$  and 2070 to 2090  $\text{cm}^{-1}$  to CO molecules adsorbed on Pt single atoms and NPs, respectively, which allowed us to compare the oxidation activity of CO molecules adsorbed at different sites and investigate the active species in supported-Pt catalyzed CO oxidation. For all the Pt samples studied, only the CO molecules adsorbed on Pt NPs could be oxidized and subsequently desorb as  $\text{CO}_2$  at reaction temperatures below 100°C. The IR peak at 2115  $\text{cm}^{-1}$ , corresponding to CO adsorbed on Pt single atoms, remained unchanged under the reaction conditions (Fig. 1, D and E, and fig. S5). This result clearly indicates the superior activity of Pt NPs compared to single atoms for CO oxidation.

The co-existence of Pt single atoms and NPs was also ob-

served in a variety of conventional, supported Pt catalysts. The IR spectra of CO adsorbed on 1 wt % Pt/ $\text{SiO}_2$ , Pt/ $\text{Al}_2\text{O}_3$  ( $\gamma$ ), Pt/ $\text{TiO}_2$  (anatase), and Pt/ $\text{ZrO}_2$  (monoclinic) at 100°C, all of which were prepared by incipient wetness impregnation and calcined at 400°C in air, are generally comprised of two types of CO bands (Fig. 2, A and B). The major CO bands centered at 2050 to 2080  $\text{cm}^{-1}$  are identical to the band from CO adsorbed on Pt NPs shown in Fig. 1A. A red-shift of the major IR bands during argon purging was observed as well (fig. S11), implying the nanoparticulate nature of the CO adsorption sites. Besides the major band, each spectrum contains one or more shoulders on the higher frequency side. The band positions of these shoulders are similar, if not identical, to the band position that we have assigned to CO molecules adsorbed on cationic Pt single atoms (within 20  $\text{cm}^{-1}$ ). These shoulder bands have been observed previously (33–35), but were ambiguously assigned to CO adsorbed on certain cationic Pt species. Based on our study with the model Pt/HZSM-5 system, we assign these bands to cationic Pt single atoms. Similar to the CO oxidation behavior that we observed on Pt/HZSM-5 samples, the CO molecules adsorbed on Pt NPs were quickly oxidized and removed upon  $\text{O}_2$  exposure, as indicated by the rapid drop in the major CO bands at 2050–2080  $\text{cm}^{-1}$  (Fig. 2, A and B, and fig. S11). Meanwhile, the bands related to CO on Pt single atoms remained unchanged regardless of the identity of the support. Thus, the IR technique can be used for identifying the two Pt species on many conventional metal oxide supports in addition to the model Pt/HZSM-5 system. The co-existence of Pt single atoms and NPs in Pt/ $\text{SiO}_2$  was further confirmed by aberration-corrected HAADF imaging, as shown in Fig. 2, C and D, and fig. S12.

Microscopy can provide only statistically limited information about the population of different Pt species. In this regard, IR spectroscopy can be used as a tool for site quantification, with a knowledge of the ratio of IR extinction coefficients for CO molecules adsorbed on Pt single atoms and NPs. To obtain this number, we quantified the respective population of Pt single atom and NP-related CO adsorption sites in Pt/ $\text{SiO}_2$  using temperature programmed oxidation (TPO) coupled with mass spectrometry (26). As shown in Fig. 2F (full spectrum and extended discussion given in figs. S13 and S14), the first sharp  $\text{CO}_2$  peak is associated with the CO molecules adsorbed on Pt NPs. The second broader  $\text{CO}_2$  peak, which extends from 150°C to 350°C, is from the CO molecules that were adsorbed on Pt single atoms, as evidenced by TPO-IR spectra (fig. S15). Based on our calculations, the CO molecules adsorbed on Pt single atoms and NPs correspond to ~11% and 10%, respectively, of the total Pt atoms in the 1 wt % Pt/ $\text{SiO}_2$  catalyst. From the peak area ratio derived from TPO-MS and IR spectra (Fig. 2, E and F) we obtain a ratio of IR extinction coefficients for CO molecules adsorbed on Pt single atoms and NPs equal to ca. 0.12. This ratio can then be used for the quantification of CO adsorption sites using IR spectroscopy.

The temperature programmed reaction (TPRx) spectra from CO oxidation with O<sub>2</sub> under continuous flow conditions over Pt/SiO<sub>2</sub> and Pt/Al<sub>2</sub>O<sub>3</sub> are shown in fig. S16. The activation energies were measured to be 90 kJ/mol and 95 kJ/mol for Pt/SiO<sub>2</sub> and Pt/Al<sub>2</sub>O<sub>3</sub>, respectively, in good agreement with the experimental and theoretical values reported for supported Pt NPs (30). The TPRx-IR spectra of Pt/SiO<sub>2</sub> (fig. S17) show negligible CO oxidation activity below 150°C, as the Pt NPs surface is dominated by CO adsorption in the presence of CO and O<sub>2</sub>. The Pt NP-related CO peak completely disappeared when the reaction temperature was increased to 160°C, accompanied with a constant formation of CO<sub>2</sub> (fig. S17). In contrast, the Pt single atom-related CO peak did not change significantly until the reaction temperature was above 200°C (figs. S15 and S17). The rapid rise of CO oxidation activity is clearly associated with the abrupt change of CO coverage on Pt NPs, which further confirms that the active sites of supported Pt in CO oxidation are Pt NPs but not single atoms.

There are two possible explanations for the distinctly different reactivity of CO molecules adsorbed on the Pt NPs and single atoms. One is the size-dependence to O<sub>2</sub> activation by Pt clusters. Small clusters have lower d-band centers, resulting in less electron back-donation to the antibonding orbital of O<sub>2</sub> molecules and thus less efficient O<sub>2</sub> activation (12).

Another possible contribution to the observed reactivity may be the binding strength of the CO molecule to the different Pt species. We conducted a series of <sup>12</sup>CO-<sup>13</sup>CO exchange experiments on the 1 wt % Pt/SiO<sub>2</sub> catalyst to probe the respective binding strengths of CO molecules on the Pt NP and single atom sites. The IR bands of <sup>13</sup>CO adsorbed on Pt single atoms and NPs both red-shift ~ 50 cm<sup>-1</sup> compared to those of <sup>12</sup>CO (Fig. 3A), consistent with reported values (28, 29). After the <sup>13</sup>CO adsorption reached an equilibrium state at 100°C, <sup>12</sup>CO was introduced to exchange with the pre-adsorbed <sup>13</sup>CO. The IR peak related to Pt NPs shifted back to 2080 cm<sup>-1</sup> in less than 30 s, indicating that the pre-adsorbed <sup>13</sup>CO on Pt NPs were rapidly replaced by <sup>12</sup>CO. In contrast, the <sup>13</sup>CO molecules adsorbed on Pt single atoms were only partially replaced by <sup>12</sup>CO even after 18 min (Fig. 3B and fig. S18). The stronger binding of CO to Pt single atoms than to Pt NPs resulted in substantially lower catalytic activity for CO oxidation.

We also examined the WGS reaction over the Pt/SiO<sub>2</sub> catalyst in order to compare the reactivity of O<sub>2</sub> and H<sub>2</sub>O with adsorbed CO, and also found that only CO molecules adsorbed on Pt NPs quickly reacted with H<sub>2</sub>O, releasing CO<sub>2</sub> (Fig. 4A). The CO molecules adsorbed on Pt single atoms remained intact upon H<sub>2</sub>O exposure at 100°C, further emphasizing the lack of activity by the Pt single atoms.

In order to better understand the origin of the promotional effect of alkali cations on Pt single atoms and NPs, we prepared a Pt-Na/SiO<sub>2</sub> catalyst with 1 wt.% Pt and a Pt/Na molar ratio of 1/3. The WGS performance of Pt/SiO<sub>2</sub> and Pt-

Na/SiO<sub>2</sub> that we have observed confirms the promotional effect of Na cations (Fig. 4C). HAADF images show a higher dispersion of Pt in the Pt-Na/SiO<sub>2</sub> case compared to the Pt/SiO<sub>2</sub> catalyst (fig. S19), in agreement with the literature results (5, 10). The IR spectra show that the addition of Na<sup>+</sup> greatly lowered the CO adsorption peak intensities, implying that Na<sup>+</sup> could reside in and block CO adsorption sites (36, 37). However, the linear and bridge CO peaks corresponding to Pt NPs of Pt-Na/SiO<sub>2</sub> are red-shifted 30 and 90 cm<sup>-1</sup>, respectively, compared to those of the Na-free sample. At a temperature up to 300°C, the introduction of H<sub>2</sub>O also only removed CO adsorbed on Pt NPs (Fig. 4B and fig. S20). Our IR data show that the promotional effect of Na<sup>+</sup> in WGS reaction mainly originates from altering the properties of Pt NPs, not single atoms. It also appears that alkali metals could lower the CO surface coverage on Pt NPs. Thus, more sites remain available for the activation of O<sub>2</sub> or H<sub>2</sub>O (17, 18).

## REFERENCES AND NOTES

- O. Korotkikh, R. Farrauto, Selective catalytic oxidation of CO in H<sub>2</sub>: Fuel cell applications. *Catal. Today* **62**, 249–254 (2000). doi:10.1016/S0920-5861(00)00426-0
- C. Ratnasamy, J. P. Wagner, Water Gas Shift Catalysis. *Catal. Rev., Sci. Eng.* **51**, 325–440 (2009). doi:10.1080/01614940903048661
- J. Kašpar, P. Fornasiero, N. Hickey, Automotive catalytic converters: Current status and some perspectives. *Catal. Today* **77**, 419–449 (2003). doi:10.1016/S0920-5861(02)00384-X
- Q. Fu, H. Saltsburg, M. Flytzani-Stephanopoulos, Active nonmetallic Au and Pt species on ceria-based water-gas shift catalysts. *Science* **301**, 935–938 (2003). Medline doi:10.1126/science.1085721
- Y. Zhai, D. Pierre, R. Si, W. Deng, P. Ferrin, A. U. Nilekar, G. Peng, J. A. Herron, D. C. Bell, H. Saltsburg, M. Mavrikakis, M. Flytzani-Stephanopoulos, Alkali-stabilized Pt-OHx species catalyze low-temperature water-gas shift reactions. *Science* **329**, 1633–1636 (2010). Medline doi:10.1126/science.1192449
- B. Qiao, A. Wang, X. Yang, L. F. Allard, Z. Jiang, Y. Cui, J. Liu, J. Li, T. Zhang, Single-atom catalysis of CO oxidation using Pt1/FeOx. *Nat. Chem.* **3**, 634–641 (2011). Medline doi:10.1038/nchem.1095
- M. Moses-DeBusk, M. Yoon, L. F. Allard, D. R. Mullins, Z. Wu, X. Yang, G. Veith, G. M. Stocks, C. K. Narula, CO oxidation on supported single Pt atoms: Experimental and ab initio density functional studies of CO interaction with Pt atom on  $\theta$ -Al<sub>2</sub>O<sub>3</sub>(010) surface. *J. Am. Chem. Soc.* **135**, 12634–12645 (2013). Medline doi:10.1021/ja401847c
- J. D. Kistler, N. Chotigkrai, P. Xu, B. Enderle, P. Praserthdam, C.-Y. Chen, N. D. Browning, B. C. Gates, A Single-Site Platinum CO Oxidation Catalyst in Zeolite KLT: Microscopic and Spectroscopic Determination of the Locations of the Platinum Atoms. *Angew. Chem. Int. Ed.* **53**, 8904–8907 (2014). doi:10.1002/anie.201403353
- E. J. Peterson, A. T. DeLaRiva, S. Lin, R. S. Johnson, H. Guo, J. T. Miller, J. Hun Kwak, C. H. Peden, B. Kiefer, L. F. Allard, F. H. Ribeiro, A. K. Datye, Low-temperature carbon monoxide oxidation catalysed by regenerable atomically dispersed palladium on alumina. *Nat. Commun.* **5**, 4885 (2014). Medline doi:10.1038/ncomms5885
- M. Yang, S. Li, Y. Wang, J. A. Herron, Y. Xu, L. F. Allard, S. Lee, J. Huang, M. Mavrikakis, M. Flytzani-Stephanopoulos, Catalytically active Au-O(OH)<sub>x</sub>-species stabilized by alkali ions on zeolites and mesoporous oxides. *Science* **346**, 1498–1501 (2014). Medline doi:10.1126/science.1260526
- F. Boccuzzi, A. Chiorino, S. Tsubota, M. Haruta, FTIR Study of Carbon Monoxide Oxidation and Scrambling at Room Temperature over Gold Supported on ZnO and TiO<sub>2</sub>. *J. Phys. Chem.* **100**, 3625–3631 (1996). doi:10.1021/jp952259n
- U. Heiz, A. Sanchez, S. Abbet, W. D. Schneider, Catalytic Oxidation of Carbon Monoxide on Monodispersed Platinum Clusters: Each Atom Counts. *J. Am. Chem. Soc.* **121**, 3214–3217 (1999). doi:10.1021/ja983616l
- D. Tibiletti, A. A. Fonseca, R. Burch, Y. Chen, J. M. Fisher, A. Goguet, C. Hardacre, P. Hu, D. Thompsett, DFT and in situ EXAFS investigation of gold/ceria-zirconia low-temperature water gas shift catalysts: Identification of the nature of the

- active form of gold. *J. Phys. Chem. B* **109**, 22553–22559 (2005). [Medline doi:10.1021/jp054576s](#)
14. A. A. Herzing, C. J. Kiely, A. F. Carley, P. Landon, G. J. Hutchings, Identification of active gold nanoclusters on iron oxide supports for CO oxidation. *Science* **321**, 1331–1335 (2008). [Medline](#)
  15. W. E. Kaden, T. Wu, W. A. Kunkel, S. L. Anderson, Electronic structure controls reactivity of size-selected Pd clusters adsorbed on TiO<sub>2</sub> surfaces. *Science* **326**, 826–829 (2009). [Medline doi:10.1126/science.1180297](#)
  16. J. H. Pazmiño, M. Shekhar, W. Damion Williams, M. Cem Akatay, J. T. Miller, W. Nicholas Delgass, F. H. Ribeiro, Metallic Pt as active sites for the water–gas shift reaction on alkali-promoted supported catalysts. *J. Catal.* **286**, 279–286 (2012). [doi:10.1016/j.jcat.2011.11.017](#)
  17. N. Pavlenko, P. P. Kostrobij, Y. Suchorski, R. Imbihl, Alkali metal effect on catalytic CO oxidation on a transition metal surface: A lattice-gas model. *Surf. Sci.* **489**, 29–36 (2001). [doi:10.1016/S0039-6028\(01\)01180-3](#)
  18. C. Pedrero, T. Waku, E. Iglesia, Oxidation of CO in H<sub>2</sub>–CO mixtures catalyzed by platinum: Alkali effects on rates and selectivity. *J. Catal.* **233**, 242–255 (2005). [doi:10.1016/j.jcat.2005.04.005](#)
  19. T. Visser, T. A. Nijhuis, A. M. van der Eerden, K. Jenken, Y. Ji, W. Bras, S. Nikitenko, Y. Ikeda, M. Lepage, B. M. Weckhuysen, Promotion effects in the oxidation of CO over zeolite-supported Pt nanoparticles. *J. Phys. Chem. B* **109**, 3822–3831 (2005). [Medline doi:10.1021/jp044767f](#)
  20. M. Kuriyama, H. Tanaka, S. Ito, T. Kubota, T. Miyao, S. Naito, K. Tomishige, K. Kunimori, Promoting mechanism of potassium in preferential CO oxidation on Pt/Al<sub>2</sub>O<sub>3</sub>. *J. Catal.* **252**, 39–48 (2007). [doi:10.1016/j.jcat.2007.09.001](#)
  21. J. M. Pigos, C. J. Brooks, G. Jacobs, B. H. Davis, Low temperature water-gas shift: Characterization of Pt-based ZrO<sub>2</sub> catalyst promoted with Na discovered by combinatorial methods. *Appl. Catal. A Gen.* **319**, 47–57 (2007). [doi:10.1016/j.apcata.2006.11.014](#)
  22. C. Yang, C. W. Garl, Infrared Studies of Carbon Monoxide Chemisorbed on Rhodium. *J. Phys. Chem.* **61**, 1504–1512 (1957). [doi:10.1021/j150557a013](#)
  23. J. T. Yates, T. M. Duncan, S. D. Worley, R. W. Vaughan, Infrared spectra of chemisorbed CO on Rh. *J. Chem. Phys.* **70**, 1219 (1979). [doi:10.1063/1.437603](#)
  24. F. Zaera, New advances in the use of infrared absorption spectroscopy for the characterization of heterogeneous catalytic reactions. *Chem. Soc. Rev.* **43**, 7624–7663 (2014). [Medline doi:10.1039/C3CS60374A](#)
  25. I. X. Green, W. Tang, M. Neurock, J. T. Yates Jr., Spectroscopic observation of dual catalytic sites during oxidation of CO on a Au/TiO<sub>2</sub> catalyst. *Science* **333**, 736–739 (2011). [Medline doi:10.1126/science.1207272](#)
  26. Materials and methods are available as supplementary materials on Science Online.
  27. W. Loewenstein. *Am. Mineral.* **39**, 92 (1954).
  28. A. Crossley, D. A. King, Infrared spectra for co isotopes chemisorbed on Pt “111”: Evidence for strong adsorbate coupling interactions. *Surf. Sci.* **68**, 528–538 (1977). [doi:10.1016/0039-6028\(77\)90245-X](#)
  29. C. W. Olsen, R. I. Masel, An infrared study of CO adsorption on Pt(111). *Surf. Sci.* **201**, 444–460 (1988). [doi:10.1016/0039-6028\(88\)90496-7](#)
  30. A. D. Allian, K. Takanebe, K. L. Furdala, X. Hao, T. J. Truex, J. Cai, C. Buda, M. Neurock, E. Iglesia, Chemisorption of CO and mechanism of CO oxidation on supported platinum nanoclusters. *J. Am. Chem. Soc.* **133**, 4498–4517 (2011). [Medline doi:10.1021/ja110073u](#)
  31. Q. Xu, Metal carbonyl cations: Generation, characterization and catalytic application. *Coord. Chem. Rev.* **231**, 83–108 (2002). [doi:10.1016/S0010-8545\(02\)00115-7](#)
  32. K. Chakarova, M. Mihaylov, K. Hadjiivanov, FTIR spectroscopic study of CO adsorption on Pt–H–ZSM-5. *Microporous Mesoporous Mater.* **81**, 305–312 (2005). [doi:10.1016/j.micromeso.2005.01.033](#)
  33. R. K. Herz, E. J. Shinouskis, Transient oxidation and reduction of alumina-supported platinum. *Appl. Surf. Sci.* **19**, 373–397 (1984). [doi:10.1016/0378-5963\(84\)90074-6](#)
  34. J. A. Anderson, Infrared study of the oxidation of carbon monoxide over Pt/Al<sub>2</sub>O<sub>3</sub>. *J. Chem. Soc., Faraday Trans.* **88**, 1197 (1992). [doi:10.1039/ft9928801197](#)
  35. F. J. Gracia, L. Bollmann, E. E. Wolf, J. T. Miller, A. J. Kropf, In situ FTIR, EXAFS, and activity studies of the effect of crystallite size on silica-supported Pt oxidation catalysts. *J. Catal.* **220**, 382–391 (2003). [doi:10.1016/S0021-9517\(03\)00296-3](#)
  36. X. L. Zhu, T. Hoang, L. L. Lobban, R. G. Mallinson, Significant Improvement in Activity and Stability of Pt/TiO<sub>2</sub> Catalyst for Water Gas Shift Reaction Via Controlling the Amount of Na Addition. *Catal. Lett.* **129**, 135–141 (2009). [doi:10.1007/s10562-008-9799-4](#)
  37. X. L. Zhu, M. Shen, L. L. Lobban, R. G. Mallinson, Structural effects of Na promotion for high water gas shift activity on Pt–Na/TiO<sub>2</sub>. *J. Catal.* **278**, 123–132 (2011). [doi:10.1016/j.jcat.2010.11.023](#)
  38. J. W. Elam, M. D. Groner, S. M. George, Viscous flow reactor with quartz crystal microbalance for thin film growth by atomic layer deposition. *Rev. Sci. Instrum.* **73**, 2981 (2002). [doi:10.1063/1.1490410](#)
  39. N. A. Ray, R. P. Van Duyne, P. C. Stair, Synthesis Strategy for Protected Metal Nanoparticles. *J. Phys. Chem. C* **116**, 7748–7756 (2012). [doi:10.1021/jp210688z](#)
  40. J. A. Libera, J. W. Elam, M. J. Pellin, Conformal ZnO coatings on high surface area silica gel using atomic layer deposition. *Thin Solid Films* **516**, 6158–6166 (2008). [doi:10.1016/j.tsf.2007.11.044](#)
  41. K. Nakanishi, *J. Porous Mater.* **4**, 67–112 (1997). [doi:10.1023/A:1009627216939](#)
  42. W. Setthapun, W. D. Williams, S. M. Kim, H. Feng, J. W. Elam, F. A. Rabuffetti, K. R. Poeppelmeier, P. C. Stair, E. A. Stach, F. H. Ribeiro, J. T. Miller, C. L. Marshall, Genesis and Evolution of Surface Species during Pt Atomic Layer Deposition on Oxide Supports Characterized by in Situ XAFS Analysis and Water–Gas Shift Reaction. *J. Phys. Chem. C* **114**, 9758–9771 (2010). [doi:10.1021/jp911178m](#)

#### ACKNOWLEDGMENTS

We acknowledge funding from the U. S. National Science Foundation CHE-1058835 (K.D., A.M.J., and P.C.S.), Northwestern University Institute for Catalysis in Energy Processes (ICEP) on Grant DOE DE-FG02-03-ER15457 (K.D., A.G., N.M.S., L.D.M., and P.C.S.). This work made use of the JEOL JEM-ARM200CF in the Electron Microscopy Service (Research Resources Center, UIC). The acquisition of the UIC JEOL JEM-ARM200CF was supported by a MRI-R2 grant from the National Science Foundation [DMR-0959470]. This work also made use of the EPIC facility and Keck- II facility of the NUANCE Center at Northwestern University, which has received support from the MRSEC program (NSF DMR-1121262) at the Materials Research Center; the International Institute for Nanotechnology (IIN); the Keck Foundation; and the State of Illinois, through the IIN. We acknowledge useful discussion with Dr. Weiqiang Wu (Northwestern University) regarding the infrared data interpretation. All data and images are available in the body of the paper or as supporting online material.

#### SUPPLEMENTARY MATERIALS

[www.sciencemag.org/cgi/content/full/science.aac6368/DC1](http://www.sciencemag.org/cgi/content/full/science.aac6368/DC1)  
Materials and Methods  
Figs. S1 to S20  
References (38–42)

23 May 2015; accepted 19 August 2015  
Published online 3 September 2015  
[10.1126/science.aac6368](https://doi.org/10.1126/science.aac6368)

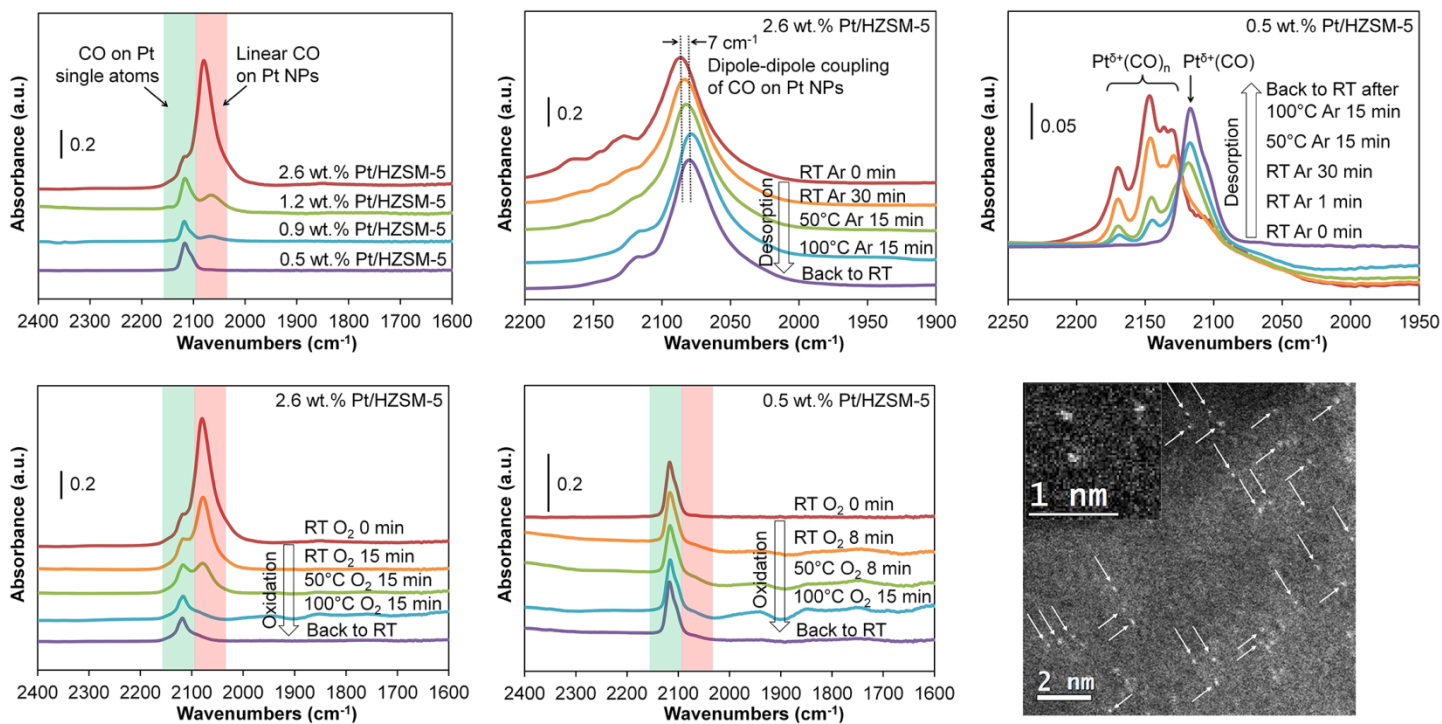


**Fig. 1. Spectroscopic and microscopic identification of Pt single atoms and NPs on HZSM-5 and SiO<sub>2</sub> (Al doped).** (A) IR spectra of CO adsorbed on different Pt/HZSM-5 after the desorption processes. Time-dependent IR spectra of CO adsorbed on 2.6 wt % Pt/HZSM-5 (B) and 0.5 wt % Pt/HZSM-5 (C) during the desorption process. Time-dependent IR spectra of CO adsorbed on 2.6 wt % Pt/HZSM-5 (D) and 0.5 wt % Pt/HZSM-5 (E) during the oxidation process. (F) HAADF image of 0.6 wt % Pt/SiO<sub>2</sub> (Al doped) with magnified image inserted and arrows to mark the single atoms.

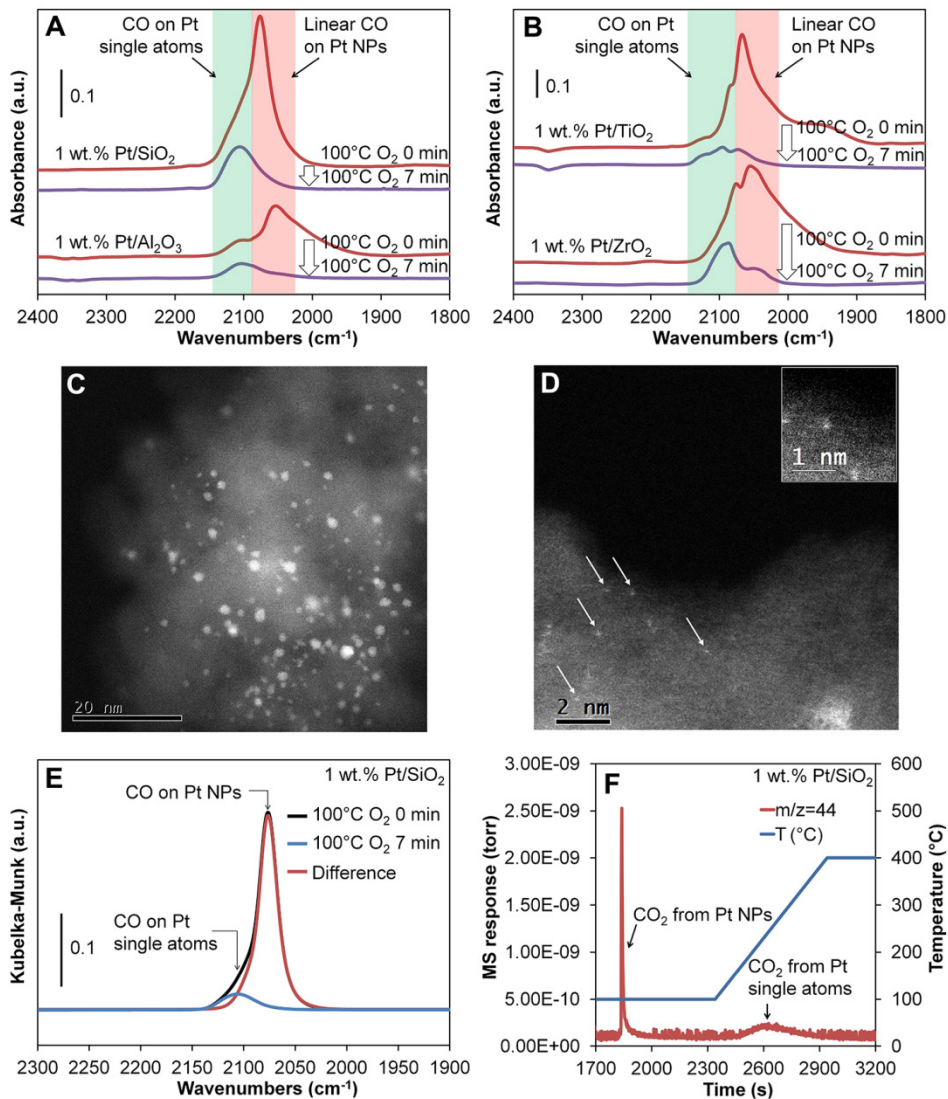


**Fig. 2. Identification and quantification of Pt single atoms and NPs on conventional supports.** IR spectra of CO adsorbed on wet-impregnated Pt/SiO<sub>2</sub> and Pt/Al<sub>2</sub>O<sub>3</sub> (**A**), Pt/TiO<sub>2</sub> and Pt/ZrO<sub>2</sub> (**B**) upon O<sub>2</sub> exposure. (**C** and **D**) HAADF images of wet-impregnated 1 wt % Pt/SiO<sub>2</sub>. The scale bars are 20 nm and 2 nm for (**C**) and (**D**), respectively with magnified image inserted in (**D**) and arrows indicating the single atoms. (**E**) IR spectra of CO adsorbed on impregnated Pt/SiO<sub>2</sub> before and after O<sub>2</sub> exposure; the difference spectrum shows the CO removed by O<sub>2</sub>; Kubelka-Munk unit is used for quantification. (**F**) CO<sub>2</sub> signal monitored by MS during the TPO process of the pre-adsorbed CO on Pt/SiO<sub>2</sub>.

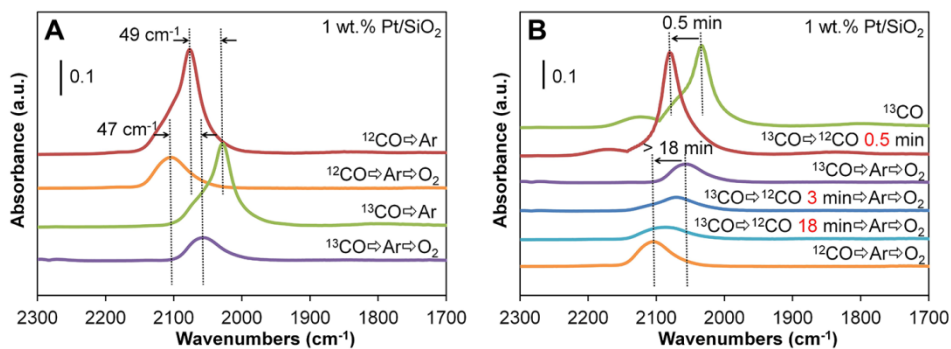


**Fig. 3.** <sup>12</sup>CO-<sup>13</sup>CO exchange on Pt/SiO<sub>2</sub>. (A) Comparison of the IR peaks of <sup>12</sup>CO and <sup>13</sup>CO adsorbed on Pt/SiO<sub>2</sub> before and after O<sub>2</sub> exposure; (B) Shift of the IR peaks at different <sup>12</sup>CO exposure time after <sup>13</sup>CO adsorption, the four spectra at the bottom were recorded after O<sub>2</sub> exposure in order to show the CO peaks related to Pt single atoms.

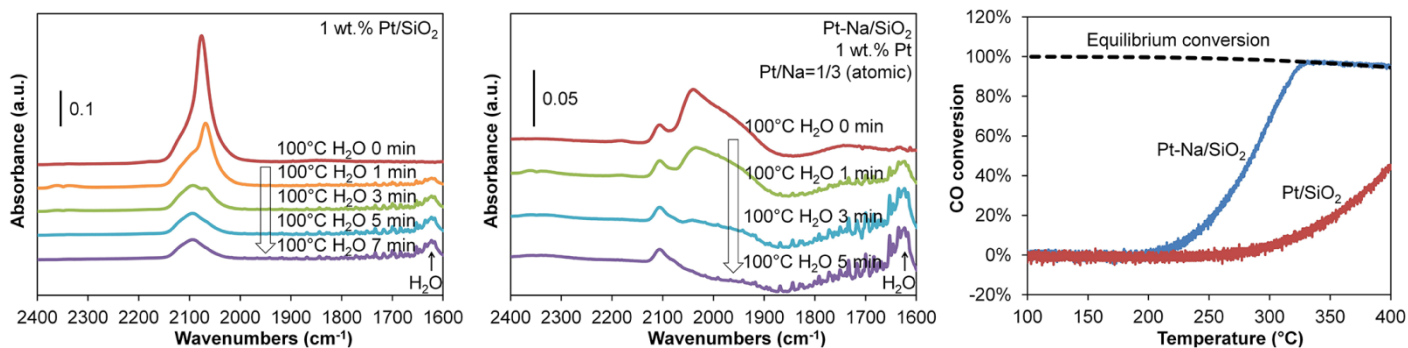


**Fig. 4.** Catalytic activity of Pt single atoms and NPs in WGS. Time-dependent IR spectra of CO adsorbed on Pt/SiO<sub>2</sub> (A) and Pt-Na/SiO<sub>2</sub> (B) upon H<sub>2</sub>O exposure. (C) Temperature programmed WGS reaction spectra over Pt/SiO<sub>2</sub> and Pt-Na/SiO<sub>2</sub>.